Biosensors and Bioelectronics 25 (2009) 475–481

Contents lists available at ScienceDirect

Biosensors and Bioelectronics

journal homepage: www.elsevier.com/locate/bios

Novel glass microprobe arrays for neural recording

Chiung-Wen Lin[a], Yu-Tao Lee[a], Chih-Wei Chang[b], Wei-Lun Hsu[c], Yen-Chung Chang[c], Weileun Fang[a,b,*]

[a] Institute of NanoEngineering and MicroSystems, National Tsing Hua University, Hsinchu 30013, Taiwan
[b] Power Mechanical Engineering Department, National Tsing Hua University, Hsinchu 30013, Taiwan
[c] Institute of Molecular Medicine, National Tsing Hua University, Hsinchu 30013, Taiwan

ARTICLE INFO

Article history:
Received 1 July 2009
Received in revised form 16 July 2009
Accepted 4 August 2009
Available online 11 August 2009

Keywords:
Neural probes
Glass microprobe
TSV
3D integration

ABSTRACT

The probe array is a useful tool for neurophysiology to detect and record neural signals. Thus, the better understanding of neural systems can be achieved. Microfabricated probes have been widely used since fine-spacing probes with well-defined electrodes in smaller footprint can be created. This study presents a novel process to realize glass 2D-microprobe array. Dielectric material like glass can provide better signal isolation capability and biocompatibility. The through silicon vias (TSVs) can also be integrated with the glass 2D-microprobe using the micromachining process. The vertical integration of chips containing glass 2D-microprobe array is realized using these silicon TSVs. The 3D-microprobe array can be easily implemented after vertical assembly of 2D-microprobe chips using bonding. In application, the 2D glass microprobe is fabricated and characterized with a low impedance of 439 kΩ at 1 kHz. The action potential of crayfish's nerve cord has successfully been recorded using the glass microprobe with peak-to-peak amplitude of 228 μV, and SNR of 46.42. The spontaneous spike of rat's cortex has also been recorded by the glass microprobe with peak-to-peak amplitude of 90 μV, and SNR of 19.72.

© 2009 Elsevier B.V. All rights reserved.

1. Introduction

The neural interface (NI) systems can be employed to create a bridge between the brain and the outside world. The NI systems draw attentions recently due to their ability to evaluate and treat the disorders of nervous system. In other words, the NI systems could be a useful rehabilitation tool for the people with paralysis (Donoghue, 2008). In general, there are three major components for NI systems: (1) a neural signals detection sensor, (2) a decoder that involves in signal processing to convert neural activity into actual command, and (3) a transducer that translates received command to action. Selecting the optimal neural signals is the primary design consideration for the detection sensor. In the nervous system with implantation NI, two types of information carrying electrical signals, including action potentials (spikes) and field potentials (FPs), can be recorded. A large amount of neural information can be carried by the recorded spikes (Donoghue, 2008). The amount of movement information like hand velocity, position, and forces can be decoded from spiking activity (Scott, 2008). Thus, the development of an action potential recording sensor is a key issue for NI systems.

The Microelectromechanical systems (MEMS) neural signal recording electrode is a promising component for NI systems in recent years. Such MEMS devices show outstanding capabilities in minimization and system integration. Thus, compared with traditional microelectrodes, the tissue damage can be reduced. Moreover, the recording ability with specified signals can be enhanced by integration with greater number of electrode sites in smaller area. The integration with complementary metal-oxide-semiconductor (CMOS) circuits is also available by means of the silicon micromachining. To date, various MEMS neural recording microelectrodes have been investigated. For instance, the flexible electrodes implemented using the polymer micromachining technology have been reported (Egert et al., 1998; Lin et al., 2009; Manos et al., 1999; Stieglitz et al., 2000). In addition, the penetrating electrodes have been extensively studied to record signals at different depths from the surface of tissue (Csicsvari et al., 2003; Najafi et al., 1985; Norlin et al., 2002; Wise et al., 1970). The aforementioned micromachined penetrating probes are planar two-dimensional (2D) structures. In order to obtain a detailed mapping of signals that transmission between neurons, the three-dimensional (3D) microprobe array is also required. The 3D silicon microprobes have been realized using the vertical etching of silicon wafer (Campbell et al., 1991; Bhandari et al., 2009). However, the numbers of electrode sites and the length of the microprobe are limited by the process. The 3D microprobe array can also be achieved by the integration of 2D microfabricated probes (Aarts et al., 2008; Hoogerwerf and Wise, 1994; Bai et al., 2000; Yao et al., 2007). However, it is

* Corresponding author at: Power Mechanical Engineering Department, National Tsing Hua University, Hsinchu 30013, Taiwan. Tel.: +886 3 574 2923; fax: +886 3 573 9372.
E-mail address: fang@pme.nthu.edu.tw (W. Fang).

0956-5663/$ – see front matter © 2009 Elsevier B.V. All rights reserved.
doi:10.1016/j.bios.2009.08.006

not straightforward to assemble the fragile microfabricated probe. Moreover, an addition silicon carrier is required for chip integration, and the electrical interconnect is also very challenge during assembly.

Most of the existing penetrating microprobes are made of single crystal silicon (SCS). According to the characteristic of semiconductor material, the single crystal silicon microprobe suffers from signal coupling during neural recording. This effect can be prevented by replacing silicon with dielectric material like polymer. However, the polymer microprobe could encounter insufficient axial or bending stiffness during penetrating. As compared to silicon, glass is suitable for signal isolation and can provide better biocompatibility (Bayliss et al., 1999). Moreover, the fracture toughness of SCS varies with different crystal planes and ranges 0.62–1.34 MPa $\times$ m$^{1/2}$ (glass is 0.77 MPa $\times$ m$^{1/2}$ by the Ferro-Ceramic Grinding Inc., 2005). The SCS microprobe could be easily broken along a particular crystal plane. Thus, development of a penetrating glass microprobe will be beneficial for neural signals recording. Presently, the high-aspect-ratio glass micromachining has rarely been investigated. The deep reactive ion etching (DRIE) of glass is regarded as a time-consuming process (Li et al., 2001; Baram and Naftali, 2006). The wafer level molding of glass is a promising technology for glass microstructure fabrication (Merz et al., 2003).

In short, the material consideration and the integration technology are two important issues for the development of microprobe array. In addition to the conventional planar electrical routing, the through-silicon via (TSV) has been exploited for vertical interconnect presently. The TSV provides the advantages of higher density and better performance for electrical interconnections. Various 3D MEMS devices have been realized under the assistant of TSV technology (Chae et al., 2008; Lin et al., 2007; Lin et al., 2008; Receveur et al., 2006). The silicon on glass MEMS devices with embedded vertical silicon vias for electrical interconnections is also reported (Lin et al., 2008). This study presents a novel process to realize 2D glass microprobe array. In addition, the silicon vias can also be integrated with the 2D glass microprobe using the micromachining process. The vertical integration of chips containing 2D glass microprobe array is realized using these silicon TSVs. Thus, the 3D microprobe array can be implemented.

2. Concept and process steps

The designs of the present 2D and 3D glass microprobe arrays are illustrated in Fig. 1. The entire structure material of the microprobe chip (including microprobe and base plate) is made from glass which has a better biocompatibility than silicon (Bayliss et al., 1999). Since glass is a dielectric material, signal crosstalk between conduction lines on top of these microprobes can be prevented. Moreover, since the environment that microprobe surrounded during tissue penetrating is conductive, dielectric material like glass can be used to prevent receiving signals from unwanted cell or neuron.

2.1. Design concept

This study presents two different microprobe designs in Fig. 1a, and these two designs can be implemented using the same microfabrication process. In the left illustration of Fig. 1a, the 2D fully glass microprobe is fabricated using the wafer level glass reflow process. A large number of recording sites can be defined on a single microprobe by using the micro fabrication process to achieve higher density recording procedure. This type of 2D glass microprobe can be used as a stand-alone device for neural recording experiment. The right figure of Fig. 1a further shows the 2D glass microprobe with embedded silicon vias for 3D integration. The low

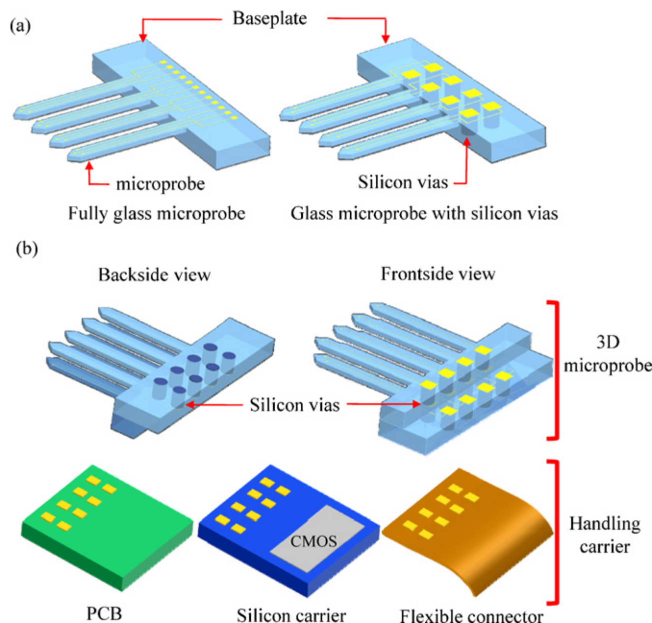

Fig. 1. Concept and integration of novel 3D glass microprobe.

resistivity silicon vias are surrounded by the glass which acts as the insulator for vias. These silicon vias are not only employed to conduct electrical signals from recording sites but also to transmit signals between the upper and the lower chips of 2D glass microprobe. Thus, the 3D glass microprobe array can be achieved by using the stacking of the 2D microprobe chips with silicon vias.

The assembly scheme of the 3D microprobe array is depicted Fig. 1b. For instance, the upper illustration in Fig. 1b shows the stacking and assembly of two 2D microprobe chips. Since each of these two microprobe chips consists of a 1×4 microprobe array, a 2×4 3D microprobe array is achieved after assembly. The 3D microprobe array can be further bonded to a handling carrier, such as the flexible connector, printed circuit board (PCB), or silicon carrier, with embedded electrical routing and even signal processing integrated circuits (IC). The upper microprobe chip contains a 1×4 silicon vias array, and the neural signals recorded by the glass microprobes of upper chip are transmitted to the lower chip through this 1×4 vias array. In addition, the lower microprobe chip contains 2×4 silicon vias array. These silicon vias receive the signals from either the upper chip vias or the lower chip microprobes, and then transmitted to the handling carrier. Thus the higher density 3D microprobe arrays can be easily implemented after the vertical assembly of 2D microprobe chips using solder. As a result, the present glass microprobe arrays has the following merits: (1) arbitrary shape of high-aspect-ratio glass microprobe can be fabricated using the present technology; (2) drawbacks like the cross-talk of sensing signals and the opto-electronic effect in silicon microprobe can be prevented; (3) embedded silicon vias enables the implementation of 3D glass microprobe array by means of the solder bonding of 2D microprobe chips.

2.2. Fabrication processes

The fabrication process illustrated in Fig. 2 has been established to implement the 2D as well as 3D glass microprobe array in Fig. 1. First, a low-resistivity silicon substrate was patterned by DRIE to act as a mold for the following wafer-level reflow-molding of glass. The silicon mold had two different depths, respectively, defining the thicknesses of microprobe and base plate. Fig. 2a shows the PECVD (plasma enhanced chemical vapor deposition) SiO_2 and photoresist

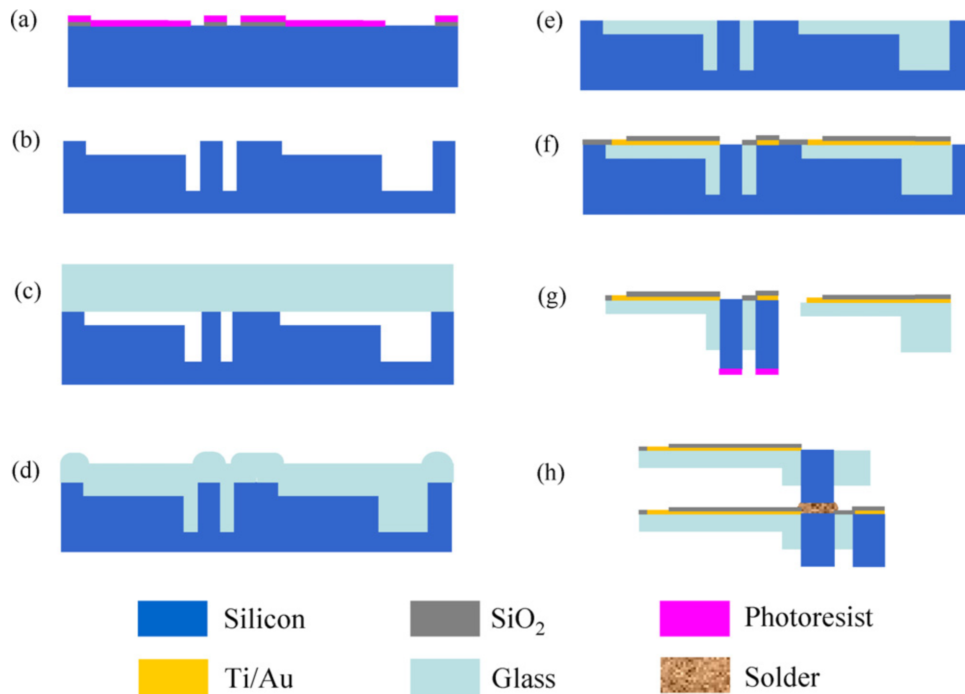

Fig. 2. Process flow for novel glass microprobe.

(AZ4620) deposited and patterned as the etching mask for DRIE. The deep trenches were defined on the silicon substrate by the first DRIE. Afterward, the photoresist etching mask was stripped and then followed by the second DRIE etching. Thus, the thicknesses of glass microprobe and the base plate were defined, as in Fig. 2b. Meanwhile, the length, width, and tip profile of microprobe were also defined by the second DRIE. As a result, the thickness of glass microprobe and base plate can be easily tuned by varying the etching conditions of DRIE.

Fig. 2c and d further shows the wafer level reflow-molding of glass performed using the silicon mold wafer. In this study, the pressure load was applied on the melted glass to perform the reflow-molding process. As shown in Fig. 2c, a Pyrex7740 glass wafer was anodic bonded to the silicon mold wafer in a vacuum chamber at the voltage of 1000 V at 400 °C. Despite the outgassing from silicon and glass wafers, the pressure inside the sealed cavity remained much smaller than the atmosphere. Thus, a large pressure load was applied on the glass suspended on top of the sealed cavity. After that, the bonded Si and Pyrex7740 glass wafers were heated at 750 °C for 7 h (Lin et al., 2008). The melted glass became viscous fluid during the heating process. By the assisting of pressure load, the melted glass was filled into the cavity, as shown in Fig. 2d. After the molding process, the wafers were cooled down to room temperature. According to (Shelby, 1997), the cooling rate of near 1 °C/min was chosen while cooling from 750 to 510 °C to reduce the thermal stress. Thus, the warpage of this Si-glass composite wafer after cooling can be minimized.

After that, a lapping process was performed to remove excessive glass until the expose of silicon via, as shown in Fig. 2e. After the lapping process, the metal thin films (Ti and Au) were deposited by evaporation and then patterned on glass microprobe for electrical routing from the electrode sites to the silicon vias, as indicated in Fig. 2f. Moreover, the PECVD SiO_2 was also deposited and patterned as the insulation layer for metal films. As shown in Fig. 2g, the backside DRIE etching of silicon wafer was performed to fully release the glass microprobe. Thus, the glass microprobe and the embedded silicon vias were implemented. As shown in Fig. 2h, the 3D microprobes array can be accomplished by stacking the chips with 2D planar microprobes and silicon vias. The conductive adhesives such as solder or silver paste were deposited onto the silicon vias. Thus, the bonding of the chips was achieved by the conductive adhesives. In addition, the vertical signal transmission of the 3D microprobe array was also accomplished by using the silicon vias and the conductive adhesives.

3. Experiment and results

To demonstrate the feasibility of this novel glass micromachining in Fig. 2, the two types of glass microprobes (with or without embedded silicon vias) illustrated in Fig. 1a are fabricated. Various tests regarding the performances of the glass microprobe, such as the impedance measurement and the neural signal recording, are also performed.

3.1. Fabrication results

The scanning electron microscopy (SEM) micrographs in Supplementary Fig. S1 show the silicon master mold prepared by the two-steps DRIE etching of Si substrate illustrated in Fig. 2b. The zoom-in micrograph in SupplementaryFig. S1 shows two different depths defined by the two-steps DRIE. The thickness of base plate defined by both of the first and the second DRIE etching is about 330 μm. The thickness of the microprobes defined by only the second DRIE etching is near 70 μm. The photo in SupplementaryFig. S2 shows the metal films deposited and patterned on the microprobe chip after completing the glass molding and lapping processes. This photo shows that various glass microprobes are embedded inside the silicon master mold wafer.

The micrographs in Fig. 3 show two different 2D glass microprobes after fully released from silicon substrate. Fig. 3a shows the typical 2D glass microprobe array with no embedded silicon vias. The photo displays the transparent glass material for microprobe, and the metal film for electrical routings and bonding pads. Moreover, the inset SEM micrograph shows the close-up view of microprobe tips with metal sensing electrodes. In this case, the

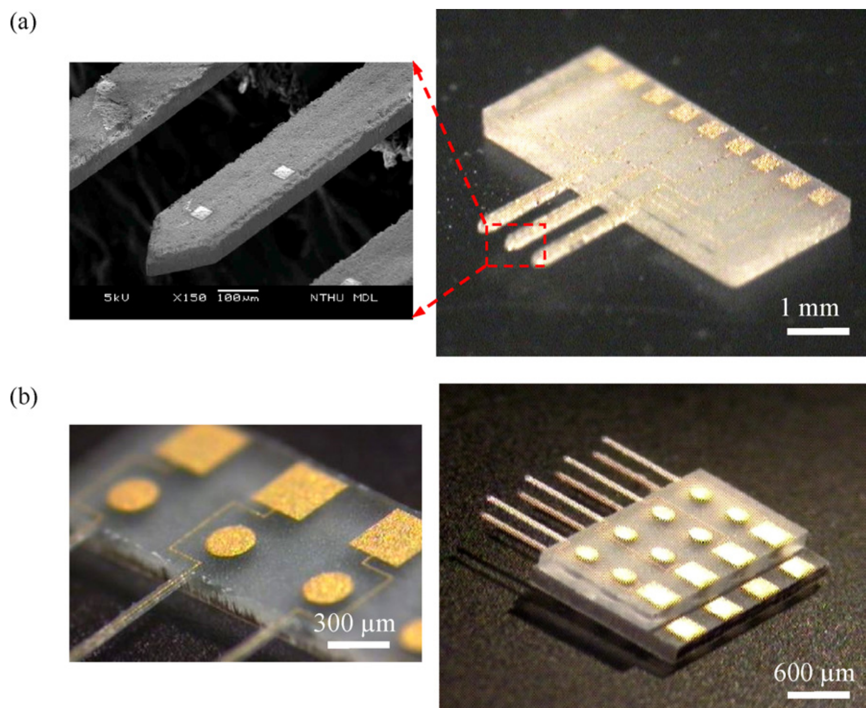

Fig. 3. Fabrication results for, (a) fully glass microprobe, (b) 3D glass microprobe with embedded silicon vias.

microprobe thickness determined by the shallow trench of Si mold is 70 μm. The photos in Fig. 3b demonstrate the assembly of two fabricated 2D glass microprobe (with 1 × 4 microprobe array) chips with embedded silicon vias. After the vertical stacking and bonding of these two 2D microprobe chips, as illustrated in Fig. 2h, the 3D glass microprobe (with 2 × 4 microprobe array) is demonstrated. The inset micrograph in Fig. 3b further displays the zoom-in view of the silicon vias inside the transparent glass, and their top metal coating.

3.2. Tests

The electric and clinic properties of the fabricated glass microprobe were evaluated by the following experiments. As to the electric property, the interface impedance of the glass microprobe was characterized by the experiment setup shown in SupplementaryFig. S3. A fully released 2D glass microprobe chip (without silicon vias) was fixed and wire bonding to a PCB handling carrier for impedance measurement, as shown in the inset of SupplementaryFig. S3. The base plate of glass microprobe was encapsulated with UV-curable polymer for insulation. The tested microprobe and Ag/AgCl reference electrode was then immersed into the phosphate-buffered saline (PBS, pH 7.4) solution. Both the glass microprobe and an the Ag/AgCl reference electrode were connected to a LCR meter (HP 4284) to extract the electrical characteristic of glass microprobe. A sinusoidal AC voltage with amplitude of 20 mV (peak-to-peak voltage) at the frequency range of 50 Hz to 10 kHz was applied to measure the interface impedance of the electrode on glass microprobe. The measured interface impedance and phase variation at different frequency is shown in the upper figure of Fig. 4. For a typical metal electrode with an open area of 2500 μm^2, the measured impedance of the present glass microprobe is 439 kΩ at 1 kHz (the typical frequency for neural recording). As a result, the ratio of impedance to electrode surface area for the glass microprobe is 0.1756 $k\Omega/\mu m^2$ (439 $k\Omega/2500\ \mu m^2$). In comparison, the ratio of impedance to electrode surface area for the silicon microprobes reported by Vetter et al. (2004) and Musa et al. (2008) are, respectively, 2.2 $k\Omega/\mu m^2$ and 0.103 $k\Omega/\mu m^2$. Thus, the present glass microprobe has reasonable impedance.

The crosstalk between the electrodes on two adjacent glass microprobes on the same probe chip has also been investigated.

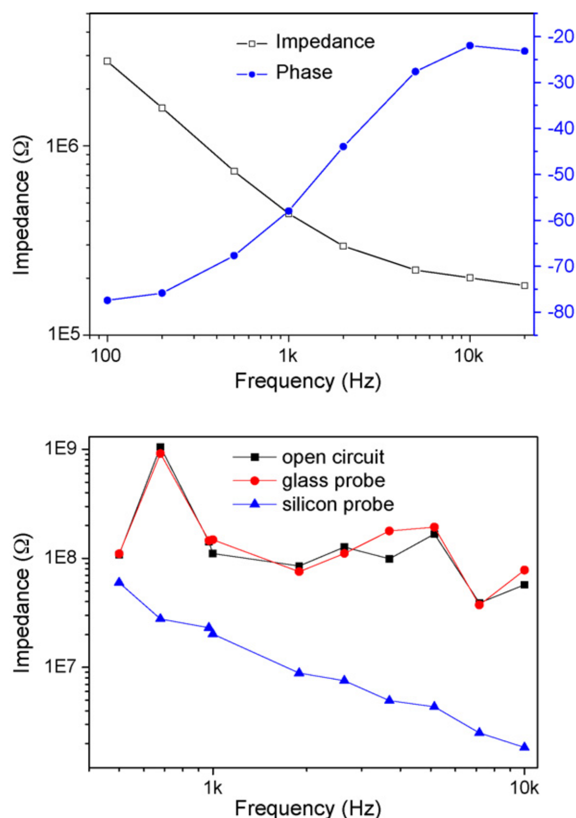

Fig. 4. Impedance measurement results of the proposed glass microprobe.

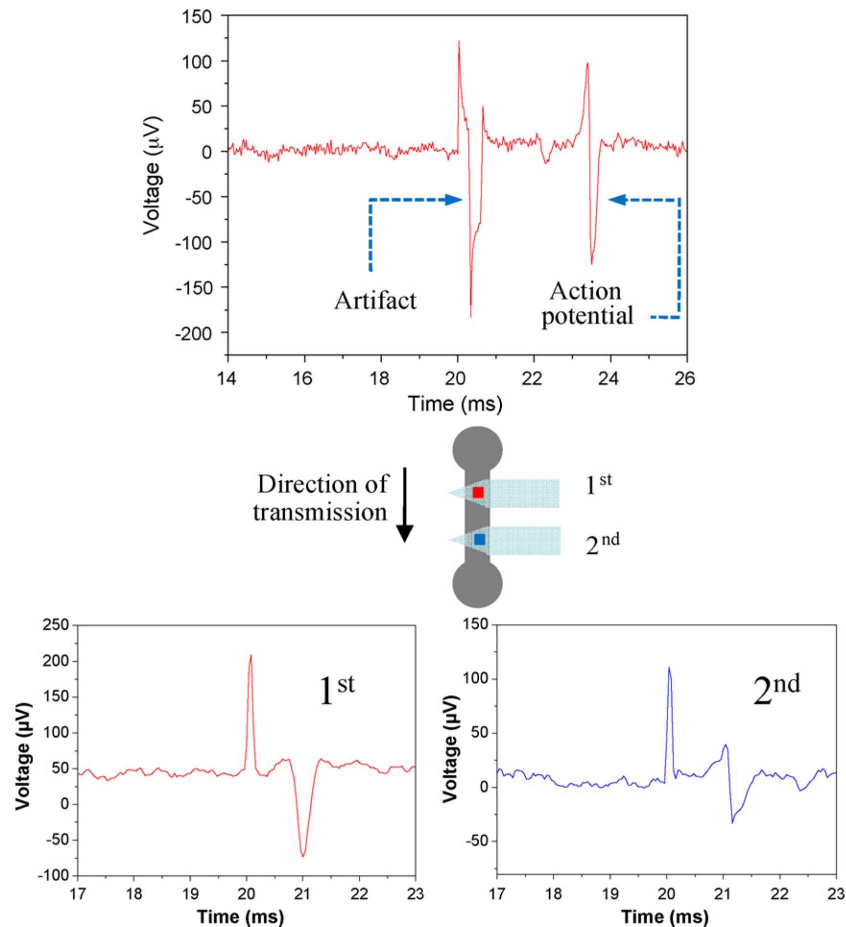

Fig. 5. Recorded action potential during extracellular recording of crayfish's nerve cord.

These two electrodes were connected to the LCR meter. In comparison, the open circuit impedance was characterized as the microprobes disconnected from the LCR meter. Moreover, the crosstalk of silicon microprobe (Wen et al., 2007) was also simultaneously characterized. The lower figure of Fig. 4, respectively shows the measured impedance of glass microprobe, silicon microprobes, and open circuit at different frequencies. The measured impedance between two shafts of microprobe is 148 MΩ at 1 kHz, while a relatively lower value was recorded by silicon (20.2 MΩ). This result indicates that a better signal isolation can be provided by the proposed glass microprobe. In addition, the measured impedance spectrum of glass microprobe is almost the same as that of the open circuit. This result confirmed the superior dielectric properties provided by the glass material.

Presently, the silicon is served as the typical material for penetrating microprobe (Csicsvari et al., 2003; Najafi et al., 1985; Norlin et al., 2002; Wise et al., 1970). As to the clinic properties of the presented glass microprobe, a biocompatibility test of the glass was performed with comparison to silicon. The primary culture from rat hippocampi was used to test the *in vitro* biocompatibility of glass (Pyrex7740) and silicon substrate. The method of primary hippocampal culture is reported in (Cheng et al., 2009). In brief, hippocampi from rat fetuses (Sprague-Dawley) at embryonic day 18 (E18) was dissected and plated at the density of 10^5 cells/ml on the following materials, glass coverslip (control), Pyrex7740 chip and silicon chip, precoated with poly-l-lysine. The cells were stained with DiI (1,1′-diocatadecyl-3,3,3′,3′-tetramethyl-indocarbocyanine perchlorate, Invitrogen) to stain cell membrane on DIV0 (days *in vitro*). On DIV3, cells were treated with 5 μM Ara-C for 1 day to curtail the growth of glial cells. Cells were kept at 37 °C under 5% CO_2 and 95% O_2 in a humidified incubator. On DIV16, the cells were fixed by 3.75% paraformaldehyde (PFA; MERCK) for 25 min and then washed with phosphate buffer saline (PBS) for 3 times. A laser scanning microscopy (LSM510, Carl Zeiss MicroImaging, Inc.) using 10× dry objective with 543 nm laser was used to excite DiI to observe neuron cells. Five non-overlapping images per chip with a field view of approximated 0.7 mm^2 were taken to count the averaged cell number per chip. SupplementaryFig.S4 shows the image and cell number with standard error ($n = 3$). The cell number of Pyrex7740 (78.1 ± 11.4 cell number/mm^2) is significantly lower than the cell number of glass coverslip (109.5 ± 3.5 cell number/mm^2). However, the cell number on Pyrex7740 (78.1 ± 11.4 cell number/mm^2) is significantly larger than that on silicon (2.9 ± 0.0 cell number/mm^2). This result shows that neuron cells are prefer to stay on the surface of Pyrex7740 than silicon. Thus, the Pyrex7740 microprobe will offer a better biocompatibility when implant into the tissue.

To evaluate the recording ability of the presented devices, the fabricated glass microprobe was employed to measure the neural signal from crayfish nerve cord and the motor cortex of rat. To prepare the sample for neural signal test, the abdomen segment of crayfish was pinned on Petri-dish filled with crayfish saline (pH 7.4, Van Harreveld and Wiersma, 1936). After that, the exoskeleton and muscle of crayfish was carefully removed to expose the ventral nerve cord. The nerve cord was then secured on the Petri-dish by insect pin. The entire experimental setup for neural signal test is illustrated in SupplementaryFig. S5. The fabricated 2D glass microprobe (with silicon vias) was wire bonded from the silicon via to the pad on PCB. Thus, the neural signal recorded from electrode was transmitted to PCB handling carrier through the silicon vias. And

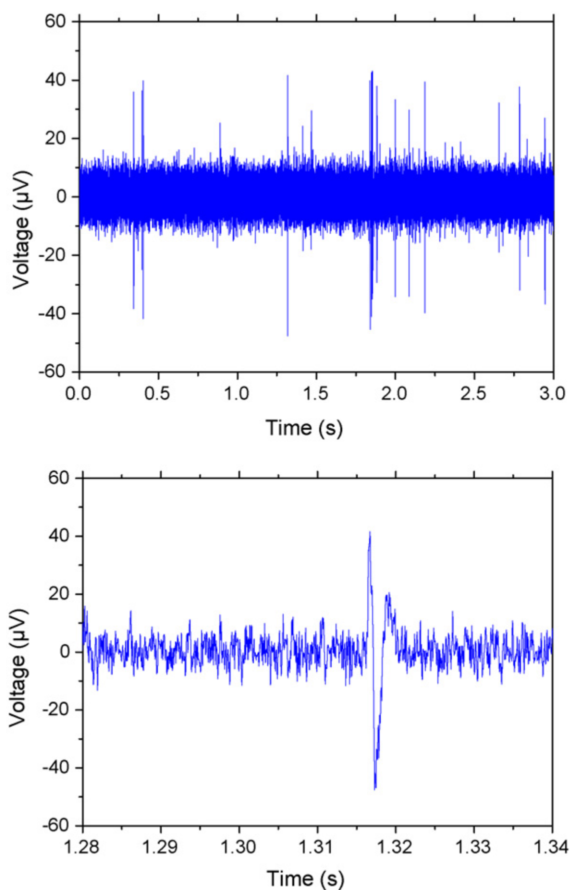

Fig. 6. Measurement results for spontaneous spikes recording of rat's cortex.

the detected neural signal was transmitted to the PCB using the silicon vias. The electrode sites of glass microprobe were in contact with the 4th abdominal segment of crayfish nerve cord. A reference electrode, made by twisted silver wire coated with Teflon, was also in contact with the 4th abdominal segment of crayfish nerve cord to simultaneously record and verified the action potential. To excite the nerve cord, a stimulation electrode, also made by twisted silver wire, was in contact with the 5th abdominal segment of crayfish nerve cord. The data acquisition software (Brain Research Center, National Tsing Hua University, Taiwan) was used to control the stimulation signal and record the neural signal. In this study, the system supplied a square wave (with 0.3 ms time duration and 5 V amplitude) to the stimulation electrode after converted by the AD/DA card (PCI-1602 ICP, DAS, Taiwan) to excite the nerve cord. The recorded signal was amplified by a four channel differential amplifier with gain 1000 (A-M systems, Model 1700) and then converted to digital signal by an AD/DA card with sampling rate at 200 kHz. The typical recorded action potential from the glass microprobe is shown in the upper figure of Fig. 5, with amplitude of 222.8 μV (peak-to-peak value; Vp-p). The signal to noise ratio (SNR) is 46.42. The definition of SNR is the ratio of Vp-p to the root mean square of the noise (Yoon et al., 2000). As a second test, the glass microprobe was employed to record the spikes propagate through the nerve cord. In this experiment, the glass microprobe array was placed and aligned on the nerve cord. Since the distance between the glass microprobes was precisely defined by the micro fabrication processes, the spike transmission rate could be calculated. For instance, as indicated in the lower figures of Fig. 5, the typical measured spike transmission time between two microprobes of distance 1200 μm is 0.16 ms. Thus, the spike transmission rate is 7.5 m/s. Those experiments data demonstrate that the recording ability of glass microprobe, and also verify the silicon vias could be use as an electrical route to carried neural signal.

The neural signal from the M1 cortex of rat was also recorded to demonstrate the recording ability of the presented glass microprobe in brain tissue. An adult rat (Wistar, male, 250 g) was used to record the neural signal. SupplementaryFig. S6 shows the recording setup. The rat was first anesthetized by pentobarbital (50 mg/kg), and then secured on the stereotaxic frame. A craniotomy was drilled on skull on the M1 location (AP: +2 mm, ML: +2.5 mm, to bregma) and the dura was also removed by forceps. The glass microprobe, mounted and wire bonded on the PCB handling carrier was connected to an eight channel headstage (Plexon Inc., Dallas, Texas) and then secured to the manipulator arm of stereotaxic frame. The glass microprobe was then gradually inserted into the M1 cortex to measure spikes from M1 neurons. The recorded signal was then amplified with gain of 20,000, digitalized, and processed and real time displayed by a multichannel acquisition processor (Plexon MAP system, Plexon Inc., Dallas, Texas). The rat was kept in anesthesia throughout the experiment. The spontaneous spikes from M1 were successfully recorded by the glass microprobe, as shown in the upper figure of Fig. 6. The lower figure of Fig. 6 further indicates the single recorded within the period of 1.31–1.32 s, and a peak-to-peak value of 89.25 μV with a SNR of 19.72 was demonstrated. The experiment results successfully show the neural signal recorded from M1 cortex of rat by the present glass microprobe, which also demonstrate the feasibility of the glass microprobe for *in vivo* tests.

4. Conclusions

A novel glass microprobe fabricated by glass reflow process is successfully demonstrated. Compared with silicon-based microprobe, better signal isolation capability and biocompatibility can be provided by the glass one. The 3D glass microprobe array has been successfully achieved by using the vertical stacking and bonding of the 2D microprobe chips. The embedded silicon vias enable the transmitting of electrical signals between each vertically-stacked 2D microprobe chip. The further integration of the 2D as well as 3D glass microprobe array on a PCB handling carrier has also been accomplished. The action potential of crayfish's nerve cord has successfully been recorded with peak-to-peak amplitude of 228 μV, and SNR of 46.42. The spontaneous spike of rat's cortex has also been recorded with peak-to-peak amplitude of 90 μV, and SNR of 19.72. The present glass microprobe also has some drawbacks and limitations. For instance, the glass reflowing is a high temperature process, thus it is not straightforward when integration with other components and processes. In addition, the planarization lapping process in Fig. 2e will lead to a rough glass surface. Although a rough surface can be exploited to reduce the interface impedance, it will also cause the disconnection of metal electrical routings. Thus, addition polishing process on glass surface is required to increase fabrication yield.

In order to achieve a more durable neural signals recording sensor for NI systems, future work will focus on the improvement of the glass microprobe. For instance, the number of electrode sites on each glass microprobe can be further increased to obtain more valuable neural signals during penetrating. More *in-vivo* tests will be performed to further evaluate the performances of the glass microprobe. Performance consistency of the glass microprobe will also be monitored regarding to the long-term implantation.

Acknowledgements

This research is sponsored in part by the NSC of Taiwan under grant of NSC-96-2627-E-007-002 and NSC-96-2628-E-007-007-

MY3. The authors would like to appreciate the Nano Facility Center of National Tsing Hua University, the NEMS Research Center of National Taiwan University, and the NSC National Nano Device Laboratory (NDL) in providing the fabrication facilities. The author also would like to thank Yung-Chen Chen and Prof. Hsin Chen of National Tsing Hua University and Prof. You-Yin Chen of National Chiao Tung University in providing the measurement facility.

Appendix A. Supplementary data

Supplementary data associated with this article can be found, in the online version, at doi:10.1016/j.bios.2009.08.006.

References

Aarts, A.A.A., Neves, H.P., Puers, R.P., Van Hoof, C., 2008. J. Micromech. Microeng. 16, 064004.
Bai, Q., Wise, K.D., Anderson, D.J., 2000. IEEE Trans. Biomed. Eng. 47, 281–289.
Baram, A., Naftali, M., 2006. J. Micromech. Microeng. 16, 2287–2291.
Bhandari, R., Negi, S., Rieth, L., Normann, R.A., Solzbacher, F., 2009. J. Micromech. Microeng. 19, 035004.
Bayliss, S.C., Buckberry, L.D., Fletcher, I., Tobin, M.J., 1999. Sens. Actuators A 74, 139–142.
Campbell, P.K., Jones, K.E., Hubert, R.J., Horch, K.W., Normann, R.A., 1991. IEEE Trans. Biomed. Eng. 38, 758–768.
Chae, J., Giachino, J.M., Najafi, K., 2008. J. Microelectromech. Syst. 17, 193–200.
Cheng, W.-Y., Hsu, W.-L., Cheng, H.-H., Huang, Z.-H., Chang, Y.-C., 2009. Anal. Biochem. 386, 105–112.
Csicsvari, J., Henze, D.A., Jamieson, B., Harris, K.D., Sirota, A., Bartho, P., Wise, K.D., Buzsaki, G., 2003. J. Neurophysiol. 90, 1314–1323.
Donoghue, J.P., 2008. Neuron 60, 511–521.
Egert, U., Schlosshauer, B., Fennrich, S., Nisch, W., Fejtl, M., Knott, T., Muller, T., Hammerle, H., 1998. Brain Res. Protocol 2, 229–242.
Ferro-Ceramic Grinding Inc., 2005. Corning Pyrex Properties, http://www ferroceramic.com/corning_table.htm (accessed May 13, 2009).
Hoogerwerf, A.C., Wise, K.D., 1994. IEEE Trans. Biomed. Eng. 41, 1136–1146.
Li, X., Abe, T., Esashi, M., 2001. Sens. Actuators A 87, 139–145.
Lin, C.-M., Lee, Y.-T., Yeh, S.-R., Fang, W., 2009. Biosens. Bioelectron. 24, 2791–2797.
Lin, C.-W., Yang, H.-A., Wang, W.C., Fang, W., 2007. J. Micromech. Microeng. 17, 1200–1205.
Lin, C.-W., Hsu, C.-P., Yang, H.-A., Wang, W.C., Fang, W., 2008. J. Micromech. Microeng. 18, 025018.
Manos, P., Pancrazio, J.J., Coulombe, M.G., Ma, W., Stenger, D.A., 1999. Neurosci. Lett. 271, 179–182.
Merz, P., Quenzer, H.J., Bernt, H., Wagner, B., Zoberbier, M., 2003. Digest of Technical Papers of Transducers'03, Boston, USA, pp. 258–261.
Musa, S., Welkenhuysen, M., Huys, R., Eberle, W., Kuyck, K., Bartic, C., Nuttin, B., Borghs, G., 2008. Proceedings of 4th Europe Conference of the International Federation for Medical and Biological Engineering, Antwerp, Belgium, pp. 2421–2425.
Najafi, K., Wise, K.D., Mochizuki, T., 1985. IEEE Trans. Electron Dev. 32, 1206–1211.
Norlin, P., Kindlundh, M., Mouroux, A., Yoshida, K., Hofmann, U.G., 2002. J. Micromech. Microeng. 12, 414–419.
Receveur, R.A.M., Zickar, M., Marxer, C., Larik, V., de Rooij, N.F., 2006. J. Micromech. Microeng. 16, 676–683.
Scott, S.H., 2008. J. Physiol. 586, 1217–1224.
Shelby, J.E., 1997. Introduction to Glass Science and Technology. The Royal Society of Chemistry, London.
Stieglitz, T., Beutel, H., Schuettler, M., Meyer, J.U., 2000. Biomed. Microdev. 2, 283–294.
Van Harreveld, A., Wiersma, C.A.G., 1936. Proc. Natl. Acad. Sci. U.S.A. 22, 667.
Vetter, R.J., Williams, J.C., Hetke, J.F., Nunamaker, E.A., Kipke, D.R., 2004. IEEE Trans. Biomed. Eng. 15, 896–904.
Wise, K.D., Angell, J.B., Starr, A., 1970. IEEE Trans. Biomed. Eng. 17, 238–247.
Wen, C.-C., Lee, Y.-T., Yeh, S.-R., Fang, W., 2007. Proc. IEEE Sens., Atlanta. USA, pp. 1128–1131.
Yao, Y., Gulari, M.N., Wiler, J.A., Wise, K.D., 2007. J. Microelectromech. Syst. 16, 977–988.
Yoon, T.H., Hwang, E.J., Shin, D.Y., Park, S.I., Oh, S.J., Jung, S.C., Shin, H.C., Kim, S.J., 2000. IEEE Trans. Biomed. Eng. 47, 1082–1087.